ruhr.paD

UA Ruhr Zentrum für
partielle Differentialgleichungen

A partition of unity approach to adaptivity and limiting in continuous finite element methods

D. Kuzmin, M.Q. de Luna and C.E. Kees

A partition of unity approach to adaptivity and limiting in continuous finite element methods

Dmitri Kuzmin[*]   Manuel Quezada de Luna[†]   Christopher E. Kees[‡]

Abstract

The partition of unity finite element method (PUFEM) proposed in this paper makes it possible to blend space and time approximations of different orders in a continuous manner. The lack of abrupt changes in the local mesh size h and polynomial degree p simplifies implementation and eliminates the need for using sophisticated hierarchical data structures. In contrast to traditional hp-adaptivity for finite elements, the proposed approach preserves discrete conservation properties and the continuity of traces at common boundaries of adjacent mesh cells. In the context of space discretizations, a continuous blending function is used to combine finite element bases corresponding to high-order polynomials and piecewise-linear approximations based on the same set of nodes. In a similar vein, spatially partitioned time discretizations can be designed using weights that depend continuously on the space variable. The design of blending functions may be based on *a priori* knowledge (e.g., in applications to problems with singularities or boundary layers), local error estimates, smoothness indicators, and/or discrete maximum principles. In adaptive methods, changes of the finite element approximation exhibit continuous dependence on the data. The presented numerical examples illustrate the typical behavior of local H^1 and L^2 errors.

Keywords: conservation laws, finite element methods, hp-adaptivity, discrete maximum principles, limiting techniques, partitioned time-stepping schemes

1   Introduction

Many advanced methods for numerical solution of partial differential equations vary the local mesh size h or the order p of polynomial approximations to capture small-scale effects and produce highly accurate predictions to the quantities of interest in an efficient manner. Prominent representatives of such high-resolution schemes include hp-adaptive finite element methods [14, 29, 32], flux-corrected transport (FCT) algorithms [27, 29, 28], and variable-order time integration schemes [16, 34].

In the process of hp-adaptation, local error indicators, smoothness sensors, and/or projections of reference solutions are employed to determine an optimal combination of h and p for each macrocell [9, 10]. Then new finite element spaces are generated using refinement or coarsening procedures which

---

[*]Institute of Applied Mathematics (LS III), TU Dortmund, kuzmin@math.uni-dortmund.de

[†]U.S. Army, ERDC-CHL, manuel.q.deluna@usace.army.mil

[‡]U.S. Army, ERDC-CHL, christopher.e.kees@usace.army.mil

typically require implementation of certain measures to preserve continuity of finite element shape functions and/or fluxes across the internal boundaries of mesh cells [5, 33]. The outcome of this adaptation procedure depends on many binary decisions and small changes of the data may produce entirely different finite element spaces. Moreover, the large number of ways in which anisotropic hp-refinement/coarsening can be performed makes it very difficult to identify the best choices.

High-resolution finite element schemes based on the FCT methodology and similar ideas [4, 20, 27, 28, 29] enforce monotonicity preservation using *limiters* to construct convex combinations of fluxes or element contributions associated with pairs of alternative approximations. This approach makes it possible to prove discrete maximum principles and existence of a solution to the nonlinear discrete problem [4, 6, 7]. In contrast to hp-FEM, algebraic limiting techniques of this kind do not change the finite element space. The formation of spurious undershoots or overshoots at nodes belonging to troubled cells is prevented by adding some artificial diffusion to a high-order approximation. The discrete nature of such corrections makes it difficult to design limiter functions that guarantee both monotonicity and optimal accuracy for problems with smooth exact solutions. In addition, the convergence behavior of iterative solvers for resulting nonlinear systems may be unsatisfactory [4, 27].

In this paper, we explore the possibility of combining pairs of finite element spaces or time-stepping schemes using globally defined *blending functions* instead of edge-based or element-based algebraic limiters defined in terms of nodal correction factors. The proposed approach formally represents a *partition of unity finite element method* (cf. [31]). It blends a space of large high-order elements $V_h^H = S_{ph,p}$, $p \geq 2$ with the space $V_h^L = S_{h,1}$ corresponding to the piecewise-linear approximation w.r.t. the same nodes. This kind of hp-adaptation preserves not only global continuity of conforming finite element spaces but also the number of local degrees of freedom per element.

The local order of the time discretization can also be adjusted using partition of unity methods. As shown in [16, 22, 23, 34], the use of space-adaptive time discretizations makes it possible to achieve stability, monotonicity, optimal accuracy, and/or discrete conservation without sacrificing other favorable properties. For example, spatially partitioned embedded Runge-Kutta methods (SPERK) [22, 23] combine complementary advantages of different time discretizations by using convex combinations of semi-discrete equations or numerical fluxes. In flux-based formulations, the degree of implicitness and order of accuracy can be locally adjusted using flux limiters [16, 23, 34]. In the present paper, we consider continuous finite element approximations in which the fluxes are defined not only on the boundaries of mesh cells but also inside. Therefore, the design of spatially partitioned time-stepping schemes calls for the use of modified flux approximations in the variational formulation. The proposed use of continuous blending functions in this context leads to handy generalizations of partitioned time integrators for finite difference and finite volume discretizations of conservation laws.

The presented numerical examples indicate that the use of high-order spatial or temporal approximations in smooth regions delivers the optimal order of accuracy in corresponding subdomains.

2 Partitioned space discretizations

Let $S_{ph,p} \subset H_0^1(\Omega) \cap C(\bar{\Omega})$ denote the space of continuous piecewise-polynomial functions such that $u_h|_K \in \mathbb{P}_p(K)$ or $u_h|_K \in \mathbb{Q}_p(K)$ for each $u_h \in S_{ph,p}$, $p \in \mathbb{N}$ and each element $K \in \mathcal{T}_{ph}$ of a conforming finite element mesh $\mathcal{T}_{ph}$. Consider a continuous high-order finite approximation $u_h^H \in S_{ph,p}$ to the solution u of an initial/boundary value problem. The corresponding *shape function* $u_h^{e,H}$ can be expressed in terms of N_{dof}^e Lagrange or Bernstein [1, 2, 24] *basis functions* $\varphi_1^{e,H}, \ldots, \varphi_{N_{\text{dof}}^e}^{e,H}$ associated with the nodal points $\mathbf{x}_1^e, \ldots, \mathbf{x}_{N_{\text{dof}}^e}^e$. A piecewise-linear or multilinear approximation $u_h^{e,L}$ based on the same set of nodes can be constructed using the $\mathbb{P}_1$ or $\mathbb{Q}_1$ Lagrange basis functions $\varphi_1^{e,L}, \ldots, \varphi_{N_{\text{dof}}^e}^{e,L}$. The superscripts H and L refer to the basis functions of the high-order and low-order finite element space, respectively. If $\varphi_i^{H,e}$ are Lagrange basis functions, then the nodal values of the shape functions $u_h^{e,H}$ and $u_h^{e,L}$ coincide. In the context of Bernstein polynomial approximations, the local basis functions $\varphi_i^{L,e}$ are associated with the nodes of the *Bèzier net* [18]. The finite element spaces

$$V_h^H = \text{span}\{\varphi_1^H, \ldots, \varphi_{N_{\text{dof}}}^H\} = S_{ph,p}$$

and

$$V_h^L = \text{span}\{\varphi_1^L, \ldots, \varphi_{N_{\text{dof}}}^L\} = S_{h,1}$$

are spanned by the same number N_{dof} of global basis functions and these basis functions are associated with the same nodes. However, the approximation properties of the spaces V_h^H and V_h^L are quite different. Adopting the design philosophy behind hp-FEM and FCT-like algebraic fixes, we would like to use the high-order approximation $u_h^{e,H}$ in 'smooth' cells and the low-order approximation $u_h^{e,L}$ in 'troubled' cells. The basis functions spanning an hp-adaptive finite element space

$$V_h(\alpha_h) := \text{span}\{\varphi_1, \ldots, \varphi_{N_{\text{dof}}}\} \subset S_{h,p+1} \tag{1}$$

can be defined by

$$\varphi_i(\mathbf{x}) = \alpha_h(\mathbf{x})\varphi_i^H(\mathbf{x}) + (1 - \alpha_h(\mathbf{x}))\varphi_i^L(\mathbf{x}), \qquad \mathbf{x} \in \bar{\Omega}, \quad i = 1, \ldots, N_{\text{dof}}, \tag{2}$$

where α_h is a blending function which yields a convex average of φ_i^H and φ_i^L. The use of a piecewise-constant basis selector ($\alpha_h^e \equiv 1$ or $\alpha_h^e \equiv 0$ in $K^e \in \mathcal{T}_{ph}$) may produce a discontinuous global approximation. Instead, we propose the use of continuous piecewise-linear blending functions

$$\alpha_h = \sum_{i=1}^{N_{\text{dof}}} \alpha_i \varphi_i^L \in V_h^L. \tag{3}$$

The partition of unity (PU) parameters $\alpha_i \in [0,1]$ may be defined using bound-preserving limiters or smoothness indicators that depend on the solution in a continuous manner, see Section 4.

If α_h is sufficiently smooth, the partitioned scheme is guaranteed to be at least as accurate as the V_h^L approximation. To show this, we consider a generic boundary value problem of the form

$$a(u,v) = b(v) \qquad \forall v \in V, \tag{4}$$

3

where $a : V \times V \to \mathbb{R}$ is a coercive and continuous linear form and $b : V \to \mathbb{R}$ is a continuous linear form on $V := H_0^1(\Omega)$. Let $u_h \in V_h(\alpha_h)$ be the solution of the discrete problem

$$a(u_h, v_h) = b(v_h) \qquad \forall v_h \in V_h(\alpha_h). \tag{5}$$

Using the Galerkin orthogonality, coercivity, and continuity, the best approximation property

$$\exists C > 0 \ \forall w_h \in V_h(\alpha_h) \quad \|u - u_h\|_{1,\Omega} \leq C \|u - w_h\|_{1,\Omega} \tag{6}$$

can be shown as in Céa's lemma. Let $w_h = \alpha_h I_{ph,p} u + (1 - \alpha_h) I_{h,1} u \in V_h(\alpha_h)$ be defined in terms of the interpolants $I_{h,1} u \in V_h^L$ and $I_{ph,p} u \in V_h^H$ such that $I_{h,1} u(\mathbf{x}_i) = u(\mathbf{x}_i) = I_{ph,p} u(\mathbf{x}_i)$ at each node $\mathbf{x}_i$ of the submesh $\mathcal{T}_h$. Suppose that $|\nabla \alpha_h(\mathbf{x})| \leq C_\alpha \in \mathbb{R}_+$ for all h and all $\mathbf{x} \in \Omega$. For any $w \in V$ we have

$$\|\alpha_h w\|_{1,\Omega}^2 = (\alpha_h w, \alpha_h w)_{0,\Omega} + (w \nabla \alpha_h + \alpha_h \nabla w, w \nabla \alpha_h + \alpha_h \nabla w)_{0,\Omega}$$
$$= \|\alpha_h w\|_{0,\Omega}^2 + \|\alpha_h \nabla w\|_{0,\Omega}^2 + (w^2, |\nabla \alpha_h|^2)_{0,\Omega} + 2(\alpha_h \nabla \alpha_h, w \nabla w)_{0,\Omega}.$$

The last term can be estimated as follows:

$$2(\alpha_h \nabla \alpha_h, w \nabla w)_{0,\Omega} = 2 \int_\Omega \alpha_h w \nabla \alpha_h \cdot \nabla w \mathrm{d}\mathbf{x} \leq 2 \int_\Omega \alpha_h |w| \, |\nabla \alpha_h| \, |\nabla w| \mathrm{d}\mathbf{x}$$
$$\leq 2 C_\alpha \int_\Omega \alpha_h \left(\frac{1}{2} |w|^2 + \frac{1}{2} |\nabla w|^2 \right) \mathrm{d}\mathbf{x} \leq C_\alpha \|w\|_{1,\Omega}^2,$$

where we have used Young's inequality and the fact that $0 \leq \alpha_h \leq 1$. It follows that

$$\|\alpha_h w\|_{1,\Omega}^2 \leq \|w\|_{0,\Omega}^2 + \|\nabla w\|_{0,\Omega}^2 + C_\alpha^2 \|w\|_{0,\Omega}^2 + C_\alpha \|w\|_{1,\Omega}^2 \leq (1 + C_\alpha)^2 \|w\|_{1,\Omega}^2.$$

Using the triangle inequality, we obtain the worst-case *a priori* error estimate

$$\|u - w_h\|_{1,\Omega} \leq \|\alpha_h(u - I_{ph,p}u)\|_{1,\Omega} + \|(1 - \alpha_h)(u - I_{h,1}u)\|_{1,\Omega}$$
$$\leq (1 + C_\alpha)(\|u - I_{ph,p}u\|_{1,\Omega} + \|u - I_{h,1}u\|_{1,\Omega}) \leq (1 + C_\alpha)(C_1 + C_p h^{p-1}) h |u|_{2,\Omega} \tag{7}$$

for $u \in H^2(\Omega)$ under usual assumptions regarding the mesh refinement strategy. The optimal order p of the high-order finite element approximation is preserved for blending functions α_h satisfying $\|(1 - \alpha_h)(u - I_{h,1}u)\|_{1,\Omega} \leq C\|\alpha_h(u - I_{ph,p}u)\|_{1,\Omega}$ for some $C > 0$. An *a priori* estimate of the global L^2 error can be obtained using the Aubin-Nitsche duality argument (see, e.g., [25]). In practice, the optimal H^1 and L^2 convergence behavior can be achieved in the core of subdomains where α_h equals 1. A numerical study of local errors for the Poisson equation is presented in Section 5.1.

3 Partitioned time discretizations

Continuous blending functions can also be used to combine time discretizations of different orders. The Galerkin finite element discretization of the time-dependent scalar conservation law

$$\frac{\partial u}{\partial t} + \nabla \cdot \mathbf{f}(u) = 0 \qquad \text{in } \Omega \subset \mathbb{R}^d, \ d \in \{1, 2, 3\} \tag{8}$$

leads a semi-discrete variational problem of the form

$$\frac{d}{dt} \int_\Omega \varphi_i u_h \mathrm{d}\mathbf{x} = \int_\Omega \nabla \varphi_i \cdot \mathbf{f}(u_h) \mathrm{d}\mathbf{x} - \int_{\partial\Omega} \varphi_i \mathbf{f}(u_h) \cdot \mathbf{n} \mathrm{d}s, \qquad i = 1, \ldots, N_{\mathrm{dof}}, \tag{9}$$

where $\mathbf{n}$ is the unit outward normal. Summing over i and using the partition of unity property

$$\sum_{i=1}^{N_{\mathrm{dof}}} \varphi_i \equiv 1 \tag{10}$$

of Lagrange and Bernstein basis functions, we find that u_h satisfies the integral conservation law

$$\frac{d}{dt} \int_\Omega u_h \mathrm{d}\mathbf{x} = - \int_{\partial\Omega} \mathbf{f}(u_h) \cdot \mathbf{n} \mathrm{d}s. \tag{11}$$

Let u_h^n denote the approximation to u_h at the discrete time level $t^n = n\Delta t$, where Δt is the time step. Introducing the blending function $\theta_h^n : \Omega \to [0,1]$, we define the convex average

$$u_h^{n+\theta} := \theta_h^n u_h^{n+1} + (1 - \theta_h^n) u_h^n \tag{12}$$

and discretize (9) in time using the following generalization of the two-level θ-scheme

$$\int_\Omega \varphi_i u_h^{n+1} \mathrm{d}\mathbf{x} = \int_\Omega \varphi_i u_h^n \mathrm{d}\mathbf{x} + \Delta t \left[\int_\Omega \nabla \varphi_i \cdot \mathbf{f}(u_h^{n+\theta}) \mathrm{d}\mathbf{x} - \int_{\partial\Omega} \varphi_i \mathbf{f}(u_h^{n+\theta}) \cdot \mathbf{n} \mathrm{d}s \right]. \tag{13}$$

The use of $\theta_h \equiv \theta \in \{0, \frac{1}{2}, 1\}$ yields the forward Euler, Crank-Nicolson, and backward Euler methods, respectively. The discrete conservation property is preserved for arbitrary blending functions since

$$\int_\Omega u_h^{n+1} \mathrm{d}\mathbf{x} = \int_\Omega u_h^n \mathrm{d}\mathbf{x} - \Delta t \int_{\partial\Omega} \mathbf{f}(u_h^{n+\theta}) \cdot \mathbf{n} \mathrm{d}s. \tag{14}$$

The proposed approach leads to a continuous finite element version of flux-based partitioned schemes for finite difference and finite volume discretizations of conservation laws [16, 23, 34]. For a comprehensive review and analysis of such schemes, we refer the reader to Ketcheson et al. [22, 23]. We envisage that similar ideas can be used to design spatially partitioned Runge-Kutta schemes for finite element discretizations. The need to invert consistent mass matrices in explicit schemes can be avoided, e.g., using deferred correction methods [1] or truncated Neumann series approximations [19, 20].

A typical application which calls for the use of a non-constant blending function θ_h in the generalized θ scheme (12),(13) is the *small cut cell problem*. Explicit schemes based on the embedded boundary cut cell methodology are subject to time step restrictions depending on the size of the smallest subcells. As shown by May and Berger [30], an implicit treatment of cut cells makes it possible to circumvent these severe time restrictions while using computationally efficient explicit time integration in regular cells. The design of such implicit-explicit (IMEX) methods is generally rather difficult due to the need to preserve consistency and conservation properties in applications to evolutionary

problems. The proposed use of continuous blending functions provides a very simple and flexible tool for combining different time discretizations in a consistent and conservative manner. The numerical study in Section 5.3 indicates that second-order overall accuracy can be achieved for $\Delta t = O(h^2)$ using a spatially partitioned θ_h scheme. Moreover, the use of $\theta_h = \frac{1}{2}$ in subdomains where rapid changes of the exact solution occur is likely to have the same positive impact on the local accuracy of temporal discretization as the use of $\alpha_h = 1$ in the context of partitioned space discretizations.

4 Design of blending functions

Optimal design of blending functions for space and time discretizations depends on the local smoothness of the solution and on the adaptation criteria. Many useful error estimation techniques and refinement strategies can be found in the literature on hp-FEM. The proposed partition of unity approach can be used to prevent violations of discrete maximum principles which are possible even for the Poisson equation if high-order finite elements are employed [12, 21]. Since the discrete Laplace operator of the piecewise-linear discretization is known to be monotone under certain restrictions on the geometric properties of mesh elements [13, 17], formation of undershoots and overshoots can be ruled out by setting $\alpha_i = 0$ at nodes of elements containing local extrema. Limiter functions based on this design criterion can be found, e.g., in [4, 6, 7, 27, 20]. In applications to hyperbolic conservation laws and anisotropic diffusion problems, discrete maximum principles can be enforced by using monotonicity-preserving artificial diffusion in $\mathbb{P}_1/\mathbb{Q}_1$ subdomains. The loss of accuracy at smooth local extrema can be avoided using continuous interpolants of nodal smoothness indicators [9, 26, 28].

5 Numerical experiments

In this section, we perform numerical studies illustrating the use of continuous blending functions as a tool for the design of adaptive finite element spaces and explicit-implicit time discretizations. In appendix A we briefly describe some details of the numerical implementation.

5.1 Poisson's equation in 2D

In the first numerical example, we study the local convergence behavior of a variable-order finite element approximation u_h to the solution of the 2D elliptic boundary value problem

$$-\Delta u = f, \qquad \text{in } \Omega,$$
$$u = 0, \qquad \text{on } \partial\Omega.$$

The domain of interest is $\Omega = (0,1)^2$. The right-hand side

$$f(x,y) = 8\pi^2 \sin(2\pi x)\sin(2\pi y)$$

of the Poisson equation is obtained by differentiating the exact solution

$$u(x,y) = \sin(2\pi x)\sin(2\pi y).$$

Let $u_h^H = u_{2h,2}$ denote the $\mathbb{Q}_2$ approximation on a uniform Cartesian mesh $\mathcal{T}_{2h}$. Then $u_h^L = u_{h,1}$ is the $\mathbb{Q}_1$ approximation on the submesh $\mathcal{T}_h$. The corresponding finite element spaces $V_h^H = S_{2h,2}$ and $V_h^L = S_{h,1}$ are combined using a blending function $\alpha_h \in V_h^L$, as defined by (3) and shown in Fig. 1(a). In this test, we use $\alpha_i = \mathrm{H}\,(x_i - 0.5)$, where $\mathrm{H} : [0,1] \to [0,1]$ is the Heaviside function defined by

$$\mathrm{H}(x) := \begin{cases} 1 & \text{if } x > 0.5, \\ \frac{1}{2} & \text{if } x = 0.5, \\ 0 & \text{if } x < 0.5. \end{cases} \tag{15}$$

The total number of degrees of freedom is $N_{\mathrm{dof}} = N_x \times N_y$, where $N_x = \frac{1}{h} + 1 = N_y$ is the number of grid lines parallel to the x- and y-axes. In Figs 1(b,c), we show the distribution of the pointwise error

$$e(x,y) = u(x,y) - u_h(x,y)$$

for the partitioned finite element approximation $u_h \in V_h(\alpha_h)$ on meshes corresponding to 321^2 and 641^2 DOFs. As expected, smaller errors are observed in the subdomain discretized using $\mathbb{Q}_2$ elements.

(a) Blending function α_h (b) Error $|e|$, $N_{\mathrm{dof}} = 321^2$ (c) Error $|e|$, $N_{\mathrm{dof}} = 641^2$
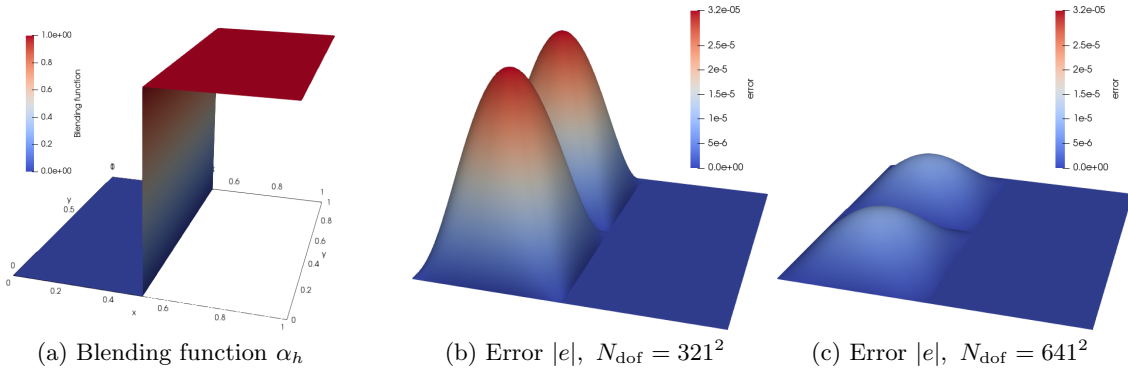
Figure 1: Blending function and error for the 2D Poisson test.

For a quantitative assessment of local errors, we compute the L^2 and H^1 norms $\|e\|_{0,D}$ and $\|e\|_{1,D}$ of the absolute error for $D = \{\Omega, \Omega_1, \Omega_2\}$, where $\Omega_1 = \{(x,y) \in \Omega \mid x < 0.5 - h\}$ and $\Omega_2 = \{(x,y) \in \Omega \mid x > 0.5 + h\}$. By definition of α_i, the $\mathbb{Q}_1$ approximation on small cells of the submesh $\mathcal{T}_h$ is used in Ω_1, whereas the $\mathbb{Q}_2$ approximation on large cells of the mesh $\mathcal{T}_{2h}$ is employed in Ω_2. A continuous transition between the corresponding finite element spaces occurs in the buffer zone $\Omega \backslash (\Omega_1 \cup \Omega_2)$. The results of a grid convergence study are shown in Table 1. Note that the optimal $\mathbb{Q}_2$ convergence rates are obtained in the subdomain Ω_2. The errors in Ω and Ω_1 exhibit the $\mathbb{Q}_1$ convergence behavior.

5.2 Steady advection-diffusion in 2D

In the second numerical example, we solve the 2D stationary advection-diffusion equation

$$\mathbf{v} \cdot \nabla u - \epsilon \Delta u = 0 \qquad \text{in } \Omega = (0,1)^2 \tag{16}$$

$N_x \times N_y$	Domain: Ω				Domain: Ω_1				Domain: Ω_2			
	$\|e\|_{0,\Omega}$		$\|e\|_{1,\Omega}$		$\|e\|_{0,\Omega_1}$		$\|e\|_{1,\Omega_1}$		$\|e\|_{0,\Omega_2}$		$\|e\|_{1,\Omega_2}$	
21^2	3.49E-3	–	2.87E-1	–	3.42E-3	–	2.83E-1	–	6.55E-4	–	4.35E-2	–
41^2	8.63E-4	2.01	1.42E-1	1.01	8.59E-4	1.99	1.42E-1	0.99	8.56E-5	2.93	1.12E-2	1.95
81^2	2.15E-4	2.00	7.12E-2	1.00	2.14E-4	1.99	7.12E-2	0.99	1.09E-5	2.97	2.84E-3	1.97
161^2	5.38E-5	2.00	3.56E-2	1.00	5.38E-5	1.99	3.56E-2	0.99	1.38E-6	2.98	7.17E-4	1.98
321^2	1.34E-5	2.00	1.78E-2	1.00	1.34E-5	1.99	1.78E-2	0.99	1.73E-7	2.99	1.79E-4	1.99
641^2	3.36E-6	2.00	8.90E-3	1.00	3.36E-6	1.99	8.90E-3	0.99	2.17E-8	2.99	4.51E-5	1.99

Table 1: Grid convergence history for the 2D Poisson test.

Following Brezzi et al. [11], we use the constant velocity field $\mathbf{v} = (1,3)$ and the diffusion coefficient $\epsilon = 0.01$. The Dirichlet boundary conditions for this test problem are given by [11]

$$u(0,y) = 1, \ \forall \ y \in [0,1],$$
$$u(x,1) = 0, \ \forall \ x \in [0,1],$$
$$u(1,y) = 0, \ \forall \ y \in [0,1],$$
$$u(x,0) = 1, \ \forall \ x \in \left[0, \frac{1}{3}\right),$$
$$u(x,0) = 0, \ \forall \ x \in \left(\frac{1}{3}, 1\right].$$

The exact solution exhibits a boundary layer and an internal layer. Once again, we combine the finite element spaces $V_h^H = S_{2h,2}$ and $V_h^L = S_{h,1}$ using a blending function $\alpha_h \in V_h^L$ such that $u_h|_K \in \mathbb{Q}_2(K)$ if $\alpha_h|_K \equiv 1$ and $u_h|_K \in \mathbb{Q}_1(K)$ if $\alpha_h|_K \equiv 0$. The $\mathbb{Q}_2$ approximation is well suited for resolving the smooth part of the parabolic internal layer but may produce undershoots or overshoots near the discontinuity point $\left(\frac{1}{3}, 0\right)$ or along the boundary $y = 1$. If the $\mathbb{Q}_1$ approximation is employed in these regions, violations of discrete maximum principles can be prevented using algebraic correction of finite element matrices [8, 27]. To show the potential benefit of using adaptive finite element spaces in this context, we define the nodal values α_i of the piecewise-linear blending function (3) as follows:

$$\alpha_i(x,y) = \begin{cases} 1, & \text{if } 2h \leq y \leq 0.8, \\ 0, & \text{otherwise.} \end{cases} \tag{17}$$

This definition produces a thin layer of pure $\mathbb{Q}_1$ elements along the inflow boundary $y = 0$ and a larger $\mathbb{Q}_1$ subdomain along the outflow boundary $y = 1$. Additionally, the $\mathbb{Q}_1$ Galerkin discretization of the advective term $\mathbf{v} \cdot \nabla u$ is stabilized by adding a discrete diffusion operator defined as in [8, 27]. The modified form of the equation corresponding to the test function $\varphi_i \in H_0^1(\Omega)$ reads

$$\sum_j (k_{ij} - d_{ij} + l_{ij})u_j = 0,$$

where $u_j = u_h(\mathbf{x}_j)$ is the nodal value at the point $\mathbf{x}_j \in \bar{\Omega}$,

$$k_{ij} = \int_\Omega \varphi_i(\mathbf{v} \cdot \nabla \varphi_j)d\mathbf{x}, \qquad l_{ij} = \epsilon \int_\Omega \nabla \varphi_i \cdot \nabla \varphi_j d\mathbf{x}$$

are the coefficients of the Galerkin discretization and

$$d_{ij} = \begin{cases} \max((\alpha_i - 1)k_{ij}, 0, (\alpha_j - 1)k_{ji}) & \text{if } j \neq i, \\ -\sum_{k \neq i} d_{ik} & \text{if } j = i \end{cases}$$

are the coefficients of the artificial diffusion operator (cf. [3, 8]). For each $\mathbf{x}_i \in \partial\Omega$, the value of $u_i = u_h(\mathbf{x}_i)$ is determined by the strongly imposed Dirichlet boundary conditions.
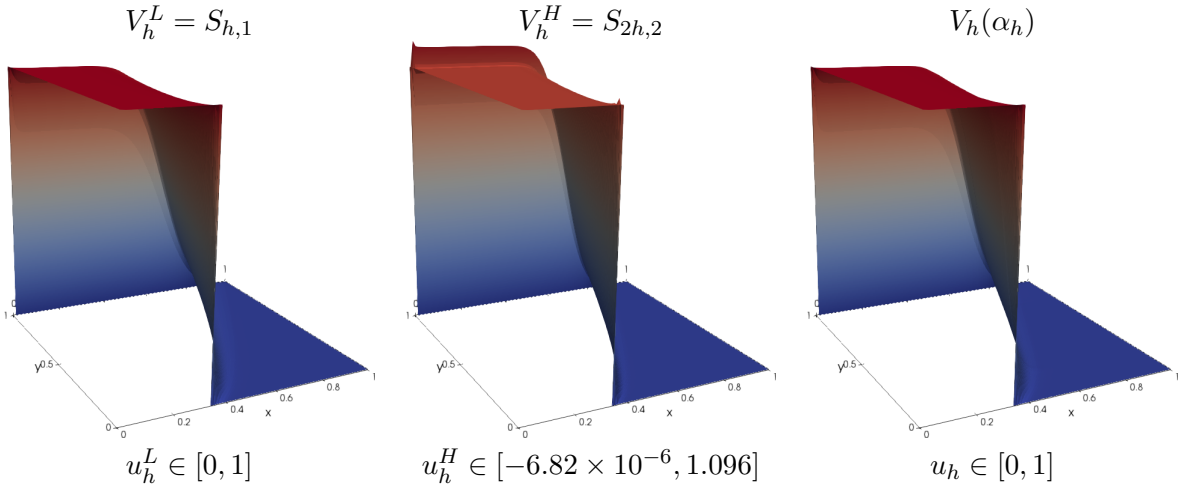
Figure 2: Solutions of the stationary advection-diffusion equation (16) obtained using finite element spaces $V_h^H = V_h(0)$, $V_h^L = V_h(1)$, and $V_h(\alpha_h)$, where α_h is the blending function defined by (17).

Computations are performed on uniform Cartesian meshes. In Figure 2, we present numerical solutions to (16) obtained using three finite element spaces of equal dimensions corresponding to $N_{\text{dof}} = N_x \times N_y = 101^2$ degrees of freedom. The pure $\mathbb{Q}_2$ approximation (u_h^H, middle panel) exhibits spurious undershoots and overshoots. A proof of the discrete maximum principle (DMP) for the pure $\mathbb{Q}_1$ approximation (u_h^L, left panel) can be found in [8]. The solution u_h shown in the right panel was calculated using the space $V_h(\alpha_h)$ with α_h defined by (17). It looks similar to u_h^L and is also bounded by the Dirichlet boundary values. This indicates that the use of $\mathbb{Q}_1$ elements and artificial diffusion operators may be restricted to small subdomains containing small-scale features that cannot be resolved properly on a given mesh. In a fully adaptive version of the proposed methodology, the nodal values of the blending function α_h may be adjusted to maximize the size of $\mathbb{Q}_2$ subdomains subject to DMP-like constraints. The development of property-preserving high-resolution finite element schemes that select appropriate values of the tuning parameters $\alpha_i \in [0, 1]$ automatically was the main motivation for preliminary numerical studies of the partition of unity method in this section.

5.3 Unsteady diffusion in 1D

To study the numerical behavior of the partitioned θ_h scheme (12),(13) in the context of embedded boundary / cut cell finite element methods, we consider the one-dimensional diffusion equation

$$\frac{\partial u}{\partial t} - d\frac{\partial^2 u}{\partial x^2} = 0 \quad \text{in } \Omega = (0, 1) \tag{18}$$

with the diffusion coefficient $d = 10^{-2}$. The exact solution is the Gaussian hill (cf. [15], p. 243)

$$u(x, t) = \frac{5}{7\sigma(t)} \exp\left\{-\left(\frac{x - 0.5}{l\sigma(t)}\right)^2\right\}, \qquad l = \frac{7\sqrt{2}}{300}, \qquad \sigma(t) = \sqrt{1 + \frac{4dt}{l^2}}. \tag{19}$$

The initial data and boundary conditions for the numerical experiment are also defined by this formula.

We discretize (18) in space using linear finite elements. Given a uniform mesh with the grid points

$$x_i = ih, \qquad h = \frac{1}{2N}, \qquad i = 0, \ldots, 2N,$$

we subdivide the two elements containing the midpoint $x_N = 0.5$ into $[0.5 - h, 0.5 - \epsilon] \cup [0.5 - \epsilon, 0.5]$ and $[0.5, 0.5 + \epsilon] \cup [0.5 + \epsilon, 0.5 + h]$, where $\epsilon = 10^{-4} \ll h$ is the size of the small cut cells.

The time step Δt is selected so that the ratio $\lambda = \frac{\Delta t}{h^2} = \frac{1}{4}$ remains constant in the process of mesh refinement. On a uniform mesh with spacing h, the forward Euler time discretization ($\theta_h \equiv 0$) is stable for $\lambda \leq \frac{1}{2}$ and second-order accurate due to the fact that $\Delta t = \lambda h^2$. However, the introduction of small cut cells makes it unstable and the code crashes for $\Delta t > \frac{1}{2}\epsilon^2$. To remedy this instability, we employ the partitioned θ scheme defined by the continuous piecewise-linear blending function

$$\theta_h(x) := \begin{cases} 1 & \text{if } |x - 0.5| \leq h, \\ 2 - \frac{1}{h}|x - 0.5| & \text{if } h \leq |x - 0.5| \leq 2h, \\ 0 & \text{if } |x - 0.5| \geq 2h. \end{cases} \tag{20}$$

That is, we use the unconditionally stable backward Euler scheme in cut cells, the forward Euler scheme in regular cells that are not adjacent to a cut cell, and a semi-implicit blend in-between.

The numerical solution presented in Fig. 3 was calculated using $h = \frac{1}{50}$ and the final time $T = 0.5$. A zoom of the cut cell subdomain is included to show how strongly the mesh size varies in this test. The errors w.r.t. the maximum norm $\|u - u_h\|_{C([0,1])} = \max_{x \in [0,1]} |u(x) - u_h(x)|$ are listed in Table 2. The partitioned θ_h scheme is stable and second-order accurate under the same time step restriction as forward Euler. At the same time, it is more efficient than backward Euler since just a few nodes are treated implicitly and the matrix of the linear system to be solved is a block-diagonal matrix.

6 Conclusions

This work indicates that the partition of unity (PU) approach to blending finite element spaces and time discretizations has significant merit in the context of hp-adaptation for conforming finite element
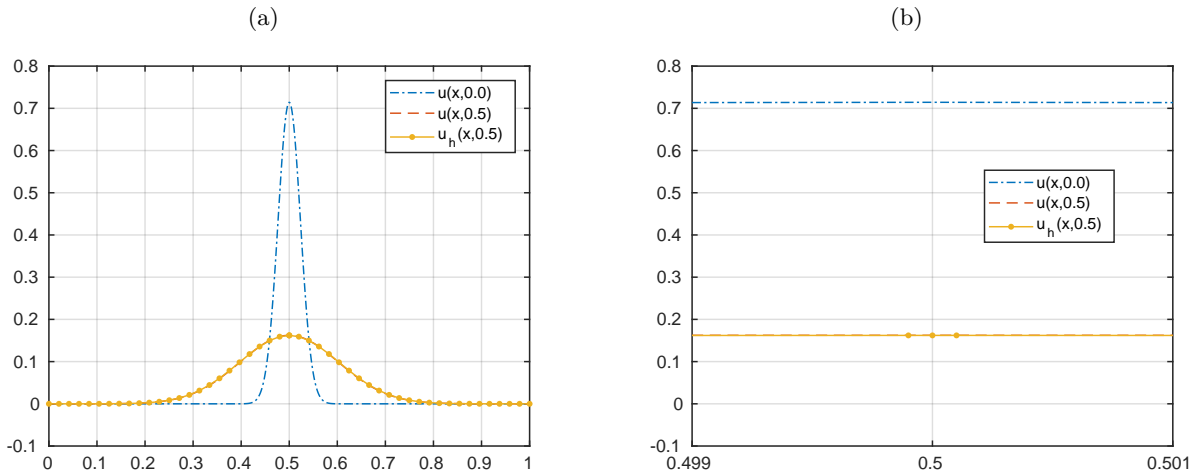
Figure 3: Diffusion of a 1D Gaussian hill: (a) numerical solution at $T = 0.5$ and (b) a zoom of the small cut cell region. $\mathbb{P}_1$ Galerkin θ_h discretization with $h = \frac{1}{50}$, $\Delta t = \frac{1}{4}h^2$.

h	$\|u - u_h\|_{C([0,1])}$	EOC
$1/100$	3.2765E-04	
$1/200$	8.6262E-05	1.93
$1/400$	2.2416E-05	1.94
$1/800$	5.5032E-06	2.03

Table 2: Diffusion of a 1D Gaussian hill: numerical errors w.r.t. the maximum norm and the experimental order of convergence for the $\mathbb{P}_1$ Galerkin θ_h discretization with $\Delta t = 0.25h^2$.

spaces and explicit-implicit partitioned time discretizations of evolutionary problems. The proposed PU hybridization of high-order basis functions with their piecewise-linear counterparts preserves global continuity of the finite element approximation as well as the number of degrees of freedom and the sparsity pattern of discrete operators. Partitioned time discretizations are well-suited for applications in which the optimal time step size (determined by stability and accuracy considerations) exhibits strong spatial variations. The use of adaptive and possibly time-dependent blending functions based on discrete maximum principles and/or local error indicators would lead to a new generation of high-resolution finite element schemes combining complementary advantages of existing hp-FEM, limiting techniques, IMEX time integrators, and local time stepping schemes. It is hoped that the present paper provides sufficient motivation for further development and analysis of such methods.

7 Acknowledgments

References

[1] R. Abgrall. High order schemes for hyperbolic problems using globally continuous approximation and avoiding mass matrices. J. Sci. Comput., 73:461–494, 2017.

[2] M. Ainsworth, G. Andriamaro, and O. Davydov. Bernstein-Bèzier finite elements of arbitrary order and optimal assembly procedures. SIAM J. Sci. Comput., 33(6):3087–3109, 2011.

[3] S. Badia and J. Bonilla. Monotonicity-preserving finite element schemes based on differentiable nonlinear stabilization. Computer Methods in Applied Mechanics and Engineering, 313:133–158, 2014.

[4] S. Badia and J. Bonilla. Monotonicity-preserving finite element schemes based on differentiable nonlinear stabilization. Computer Methods Appl. Mech. Engrg., 313:133–158, 2017.

[5] W. Bangerth and O. Kayser-Herold. Data structures and requirements for hp finite element software. ACM Transactions on Mathematical Software, 36:4/1–4/31, 2009.

[6] G. Barrenechea, V. John, and P. Knobloch. Analysis of algebraic flux correction schemes. SIAM J. Numer. Anal., 54(4):2427–2451, 2016.

[7] G. Barrenechea, V. John, and P. Knobloch. A linearity preserving algebraic flux correction scheme satisfying the discrete maximum principle on general meshes. Mathematical Models and Methods in Applied Sciences (M3AS), 27(3):525–548, 2017.

[8] G. R. Barrenechea, V. John, and P. Knobloch. Analysis of algebraic flux correction schemes. SIAM J. Numer. Anal., 54(4):2427–2451, 2016.

[9] M. Bittl and D. Kuzmin. An hp-adaptive flux-corrected transport algorithm for continuous finite elements. Computing, 95(1):S27–S48, 2013.

[10] M. Bittl and D. Kuzmin. The reference solution approach to hp-adaptivity in finite element flux-corrected transport algorithms. In I. Lirkov, S. Margenov, and J. Wasniewski, editors, Large Scale Scientific Computing, pages 197–204. Springer, 2014.

[11] F. Brezzi, L. Marini, and A. Russo. On the choice of a stabilizing subgrid for convection–diffusion problems. Computer Methods in Applied Mechanics and Engineering, 194(2-5):127–148, 2005.

[12] T. Brunner. Preserving positivity of solutions to the diffusion equation for higher-order finite elements in under resolved regions. Technical Report LLNL-PROC-66674, Lawrence Livermore National Laboratory, 2015.

[13] P. Ciarlet and P.-A. Raviart. Maximum principle and convergence for the finite element method. Comput. Methods Appl. Mech. Engrg., 2(1):17—31, 1973.

[14] L. Demkowicz. Computing with hp-Adaptive Finite Elements. Chapman & Hall/CRC, 2006.

[15] J. Donea and A. Huerta. Finite Element Methods for Flow Problems. John Wiley & Sons, 2003.

[16] K. Duraisamy, K. Baeder, and J.-G. Liu. Concepts and application of time-limiters to high resolution schemes. J. of Sci. Comput., 19:139–162, 2003.

[17] I. Faragó, R. Horváth, and S. Korotov. Discrete maximum principle for linear parabolic problems solved on hybrid meshes. Appl. Numer. Math., 53:249–264, 2005.

[18] T. N. T. Goodman. Further variation diminishing properties of Bernstein polynomials on triangles. Constructive Approximation, 3:297–305, 1987.

[19] J.-L. Guermond and R. Pasquetti. A correction technique for the dispersive effects of mass lumping for transport problems. Computer Methods Appl. Mech. and Engrg., 253(1):186–198, 2013.

[20] J.-L. Guermond, M. Nazarov, B. Popov, and Y. Yang. A second-order maximum principle preserving lagrange finite element technique for nonlinear scalar conservation equations. Mathematical Models and Methods in Applied Sciences (M3AS), 52(4):2163–2182, 2014.

[21] W. Höhn and H. Mittelmann. Some remarks on the discrete maximum principle for finite elements of higher order. Computing, 27(2):145—154, 1981.

[22] W. Hundsdorfer, D. I. Ketcheson, and I. Savostianov. Error analysis of explicit partitioned Runge-Kutta schemes for conservation laws. J. Sci. Comput., 63:633–653, 2015.

[23] D. I. Ketcheson, C. B. MacDonald, and S. J. Ruuth. Spatially partitioned embedded Runge-Kutta methods. SIAM J. Numer. Anal., 51(5):2887–2910, 2013.

[24] R. C. Kirby. Fast simplicial finite element algorithms using Bernstein polynomials. Numer. Math., 117(4):3087–3109, 2011.

[25] P. Knabner and L. Angermann. Numerical Methods for Elliptic and Parabolic Partial Differential Equations. Springer, 2003.

[26] D. Kuzmin and F. Schieweck. A parameter-free smoothness indicator for high-resolution finite element schemes. Central European Journal of Mathematics, 11(8):1478–1488, 2013.

[27] D. Kuzmin, R. Löhner, and S. Turek. Flux-Corrected Transport: Principles, Algorithms, and Applications. Scientific Computation. Springer, 2012.

[28] C. Lohmann, D. Kuzmin, J. Shadid, and S. Mabuza. Flux-corrected transport algorithms for continuous Galerkin methods based on high order Bernstein finite elements. J. Comput. Phys., 344(1):51–186, 2017.

[29] R. Löhner. Applied CFD Techniques: An Introduction Based on Finite Element Methods. John Wiley & Sons, 2008.

[30] S. May and M. Berger. An explicit implicit scheme for cut cells in embedded boundary meshes. Journal of Scientific Computing, 71(3):919–943, 2017.

[31] J. M. Melenk and I. Babuška. The Partition of Unity Finite Element Method: Basic theory and applications. Computer Methods in Applied Mechanics and Engineering, 139(1-4):289–314, 1996.

[32] P. Solin, K. Segeth, and I. Dolezel. Higher-Order Finite Element Methods. Chapman and Hall / CRC Press, 2003.

[33] P. Solin, J. Cerveny, and I. Dolezel. Arbitrary-level hanging nodes and automatic adaptivity in the hp-FEM. Math. Comput. Simul., 77:117 – 132, 2008.

[34] P. van Slingerland, M. Borsboom, and C. Vuik. A local theta scheme for advection problems with strongly varying meshes and velocity profiles. Technical Report 08-17, Department of Applied Mathematical Analysis, Delft University of Technology, 2008.

A   Numerical implementation

In this Appendix, we provide brief details about the numerical implementation of the adaptive space discretization proposed in §2. The space $V_h(\alpha_h)$ is easy to implement in a standard finite element code if the same data structures are employed for all spaces. This natural implementation strategy implies that the contributions of $S_{2h,2}$ and $S_{h,1}$ use the same mappings, the same numbering of degrees of freedom etc. Note that the sparsity patterns of finite element matrices corresponding to the $S_{2h,2}$ and $S_{h,1}$ approximations are different. Indeed, the $S_{2h,2}$ matrices have more non-zero entries than their $S_{h,1}$ counterparts. For any nontrivial choice of the blending function α_h, the sparsity pattern of the space $V_h(\alpha_h)$ is the same as that of $S_{2h,2}$. Therefore, it is worthwhile to use the extended $S_{2h,2}$ connectivity matrix for the contribution of the space $S_{h,1}$ as well. Then the size of the $V_h(\alpha_h)$ element matrices and the data structures for indirect addressing will be the same as in the case of a pure $S_{2h,2}$ approximation even if the compact-stencil $S_{h,1}$ subcell approximation is employed in some cells.

The use of common data structures facilitates blending of the two spaces and makes it possible to perform operations with global degrees of freedom directly without any kind of index mapping. In the present 2D implementation, we use quadrilateral elements. The local basis functions for $S_{h,1}$ and $S_{2h,2}$ are defined as tensor products of piecewise-linear and quadratic polynomials on the common one-dimensional reference element, see Fig. 4. Using standard mappings from the reference element to physical cells, we construct 9 biquadratic functions $\varphi_i^{e,H}$ and 9 piecewise-bilinear basis functions $\varphi_i^{e,L}$ on each quadrilateral cell of the mesh $\mathcal{T}_{2h}$. Then standard finite element procedures are invoked to generate element matrices/vectors and perform element-by-element assembly.

When it comes to combining the spaces $V_h^H = S_{2h,2}$ and $V_h^L = S_{h,1}$ using a blending function $\alpha_h \in V_h^L$, we need to evaluate the partitioned basis functions $\varphi_i^e = \alpha_h \varphi_i^{e,H} + (1 - \alpha_h)\varphi_i^{e,L}$ and their derivatives at the quadrature points. Note that the value of $\varphi_i^e(\mathbf{x})$ is an easily computable convex combination of $\varphi_i^{e,H}(\mathbf{x})$ and $\varphi_i^{e,L}(\mathbf{x})$. However, the partial derivatives of φ_i depend on the gradient of α_h which is defined only on subcells, i.e., on elements of the submesh $\mathcal{T}_h$ on which the basis functions φ_i^L are continuous bilinear polynomials. To avoid a loss of accuracy due to numerical integration of discontinuous functions on elements of the mesh $\mathcal{T}_{2h}$, we map each subcell to a subcell of the reference element, perform numerical integration on subcells using standard quadrature and the Jacobian of the subcell mapping, and add the resulting subcell contribution to the element matrix/vector in the same way in which element contributions are inserted into global matrices/vectors. The use of composite quadrature on subcells makes it possible to integrate the gradients of $\varphi_i(\alpha_h)$ exactly and is a prerequisite for achieving optimal convergence with partitioned $V_h(\alpha_h)$ spaces.
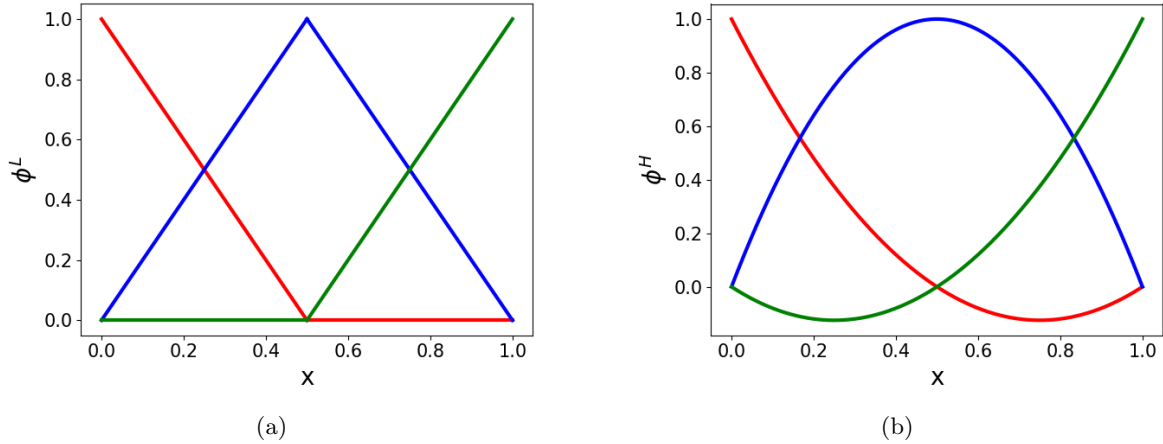

(a)

(b)

Figure 4: Definition of (a) piecewise-linear and (b) quadratic basis functions on the same one-dimensional reference element.